Heading-Error-Free Optical Atomic Magnetometry in the Earth-Field Range

Rui Zhang,[1,2,3] Dimitra Kanta,[2,3] Arne Wickenbrock,[2,3] Hong Guo,[1,*] and Dmitry Budker[2,3,4,†]
[1]State Key Laboratory of Advanced Optical Communication Systems and Networks, Department of Electronics, and Center for Quantum Information Technology, Peking University, Beijing 100871, China
[2]Johannes Gutenberg-Universität Mainz, 55128 Mainz, Germany
[3]Helmholtz-Institut Mainz, GSI Helmholtzzentrum für Schwerionenforschung, 55128 Mainz, Germany
[4]Department of Physics, University of California, Berkeley, California 94720, USA

(Received 18 April 2022; revised 19 January 2023; accepted 1 March 2023; published 12 April 2023)

We demonstrate an alignment-based ^{87}Rb magnetometer that is immune to nonlinear Zeeman (NLZ) splitting, addressing an important problem in alkali-metal atomic magnetometry. In our scheme, there is a single magnetic resonance peak and well-separated hyperfine transition frequencies, making the magnetometer insensitive or even immune to NLZ-related heading errors. It is shown that the magnetometer can be implemented for practical measurements in geomagnetic environments, and the photon-shot-noise-limited sensitivity reaches 9 fT/$\sqrt{\text{Hz}}$ at 5 μT and remains at tens of fT/$\sqrt{\text{Hz}}$ at 50 μT at room temperature.

DOI: 10.1103/PhysRevLett.130.153601

Sensitive magnetometry in the Earth-field range is important in various applications—for example, geophysical exploration [1–4], biomagnetic field detection [5,6], fundamental physics experiments [7] searching for dark matter [8–10], *CP*-violating electric dipole moments [11] and spin-dependent exotic interactions [12,13], and magnetic field standards [14,15]. Scalar alkali-metal atomic magnetometers, which are based on measuring the Zeeman splitting of an alkali-metal ground state, are attractive for such tasks because of their high sensitivity, reaching the fT/$\sqrt{\text{Hz}}$ level, and cryogen-free operation [16–20]. However, heading error—i.e., the dependence of the (nominally scalar) magnetometer reading on the direction of the magnetic field, which is often at the nT level and is several orders of magnitude larger than the state-of-art sensitivity for 1 Hz bandwidth (∼fT)—introduces motion-related noise for mobile-platform-borne or wearable systems [17]. Even when the magnetometer is at motional rest, there are heading-error-related systematic errors that depend on various experimental parameters—e.g., light power and frequency—reducing the long-term stability (accuracy) that is important for fundamental physics [21].

Depending on the type of the atomic sensor, there are mainly three physical sources of heading error: a major one is the nonlinear Zeeman effect (NLZ) due to the coupling between electron spin and nuclear spin [22–24], and the other two are the different gyromagnetic ratios of the two ground hyperfine states due to the nuclear Zeeman effect (NuZ) [24,25], and the magnetic-field-direction-dependent light shift (LS) [23]. The first two effects lead to the direction-dependent asymmetry of the magnetic resonance curve, and the third one leads to the direction-dependent shift of the magnetic resonance frequency. The NLZ and LS effects are also the source of alignment-to-orientation conversion [26,27].

There are three common strategies to suppress the NLZ-related heading error: (1) physical or theoretical compensation, including compensation with tensor light shift [28], compensation with spatially separated pumping beams of opposite circular polarizations [23], and using a high-power pump and correcting with theoretical predictions [24,29]; (2) using modulation schemes to address atomic spins in states less sensitive to direction-related magnetic resonance asymmetry, including synchronous optical pumping with double modulation [30], push-pull pump [31], and spin-locking with synchronous optical pumping and a radio-frequency (RF) [22] or modulated optical [32] field; and (3) using transitions intrinsically free from NLZ-related splitting—for example, the excitation of high-order atomic polarization moments [33]. Compared with the first two strategies, whose performance relies on the careful adjustment of experimental parameters, theoretically, the latter strategy should give a better heading-error suppression, as it is intrinsically free from the NLZ effect, and it does not require special hardware or additional modulation, which is especially welcome for mobile or wearable systems. However, these approaches suffer from a dramatic decrease of signal amplitude in the geomagnetic field range, which precludes their applications in high-sensitivity magnetometry.

Here, we show an alternative all-optical ^{87}Rb magnetometer which is intrinsically free from the NLZ-related heading error, with the heading error due to the NuZ and LS effects being largely suppressed at the same time. It retains the NLZ-splitting-free property and simplicity of the above third strategy, while allowing for high sensitivity.

Experiments with a room-temperature vapor cell demonstrate a photon-shot-noise-limited sensitivity of tens of $\mathrm{fT}/\sqrt{\mathrm{Hz}}$ in the geomagnetic field range. Instead of using the magnetic resonance between the stretched states [33], the magnetometry technique developed here is based on the alignment magnetic resonance of the $5^2S_{1/2}F = 1$ state of ^{87}Rb. As there is only a single alignment magnetic resonance in the $F = 1$ ground hyperfine state, corresponding to the transition between the $F = 1$, $m = 1$ and $F = 1$, $m = -1$ states [34], magnetometry based on this resonance is free from the NLZ-related splitting and asymmetry of the magnetic resonance curve, and thus is intrinsically free from NLZ-related heading error. The higher efficiency to produce and detect alignment (quadrupole moment) than higher-order polarization moments, such as the hexadecapole moment [33], enables highly sensitive magnetometry in the geomagnetic field range.

This scheme is also good at suppressing the heading error due to the NuZ and LS effects. The fully resolved ground hyperfine states in the antirelaxation-coated cell enable individual addressing of the desired $5^2S_{1/2}F = 1$ hyperfine state, suppressing the NuZ-related heading error to at most the tens of fT level. Besides this, the use of linearly polarized pump and probe beams largely suppresses the vector light shift of the $F = 1$ alignment magnetic resonance. The only light shift comes from the Zeeman-shift-related unbalanced detuning of optical transitions involving, respectively, the $F = 1$, $m = 1$ and $F = 1, m = -1$ states and the imperfect polarization of the light. An advantage of the presently introduced method for heading-error suppression for practical implementation is its particular simplicity: no special hardware or additional modulation is required.

The NLZ effect of an alkali ground state, such as the $5^2S_{1/2}$ state for ^{87}Rb shown in Fig. 1(a), is described by the Breit-Rabi formula [35]. The energies of Zeeman sublevels have a nonlinear dependence with respect to the magnetic field strength, and thus, the intervals between adjacent Zeeman sublevels become unequal as the field increases. As a result, in the $F = 2$ ($F = 1$) hyperfine state, there are four (two) different $\Delta m = 1$ magnetic resonance frequencies, which leads to asymmetric broadening or splitting of the magnetic resonance curve when the background field is in the geomagnetic field range [22–24]. As the populations and transition matrix elements for different Zeeman sublevels change with the magnetic-field direction, the amplitudes of different components of the magnetic resonance change as well, which leads to the magnetic-field-direction-dependent asymmetry of the overall magnetic resonance and gives rise to heading errors [22–24]. In contrast to the $\Delta m = 1$ magnetic resonance, there is only a single $\Delta m = 2$ resonance in the $F = 1$ hyperfine state. Such a single magnetic resonance is intrinsically free from the NLZ-related splitting and asymmetry of the resonance curve, and thus is free from the NLZ-related heading error.

In order to generate and measure atomic polarization in the $F = 1$ hyperfine state [see Fig. 1(b)], we pump with 795 nm laser light resonant with the ^{87}Rb D1 transition ($5^2S_{1/2}F = 2 \rightarrow 5^2P_{1/2}F' = 2$) and probe with 780 nm laser light tuned to the low-frequency side of the ^{87}Rb D2 transition (about 0.5 GHz from the $5^2S_{1/2}F = 1 \rightarrow 5^2P_{3/2}F'' = 0$ transition). The pump beam generates atomic polarization in the $F = 1$ state via repopulation pumping [36], and the polarization is monitored by detecting the optical rotation of the probe light. To achieve magnetic resonance, the pump beam is modulated at 2 times the Larmor frequency of the $F = 1$ hyperfine state. In the geomagnetic field range, the splitting between the $F = 1$ and $F = 2$ resonance frequencies is in the kHz range; see Fig. S2 in the Supplemental Material [37]. As this splitting is much larger than the relaxation rate of the ground-state polarization, the $F = 2$ state will not be trapped in the dark state, and the pumping process is efficient. Since the pump and probe beam are resonant with transitions starting from different ground hyperfine states, such a technique constitutes indirect pumping which does not cause power broadening of the magnetic resonance [38,39].

The experimental arrangement for measuring the alignment magnetic resonance is shown in Fig. 1(c). The cylindrical antirelaxation-coated atomic vapor cell has a diameter of about 4 cm and a length of about 5 cm, filled with isotope-enriched ^{87}Rb. Both the pump and the probe beam are linearly polarized and propagate through the atomic vapor cell along the z direction. The pump beam is square-wave modulated with an acousto-optic modulator (AOM) at around 2 times the Larmor frequency, with a duty cycle of 20%. The corresponding alignment magnetic resonances with a background magnetic field set along the z axis are shown in Fig. 2(a). We also built an orientation-magnetic-resonance setup to compare the alignment and orientation resonances, as shown in Fig. 1(d). The pump (probe) beam is circularly (linearly) polarized and propagates through the atomic vapor cell along the y (x) direction. In this case, the pump beam is square-wave modulated with a duty cycle of 20% at around the Larmor frequency. The orientation magnetic resonances with a background magnetic field set along the z axis are shown in Fig. 2(b). In order to maintain the consistency of experimental conditions, the two setups share the same vapor cell, and the pump and probe beams of these two setups are derived from the same pump and probe lasers, respectively.

A comparison of the magnetic field dependence of alignment and orientation magnetic resonances is shown in Fig. 2, in which the background magnetic field is set along the z direction, with strength varying from 20 μT to 50 μT (data are shifted vertically for clarity). The time-averaged optical power of the pump and probe beam in the alignment (orientation) experiment are 100 μW (50 μW) and 300 μW (15 μW), respectively. These parameters are chosen to produce relatively strong signals with minimal

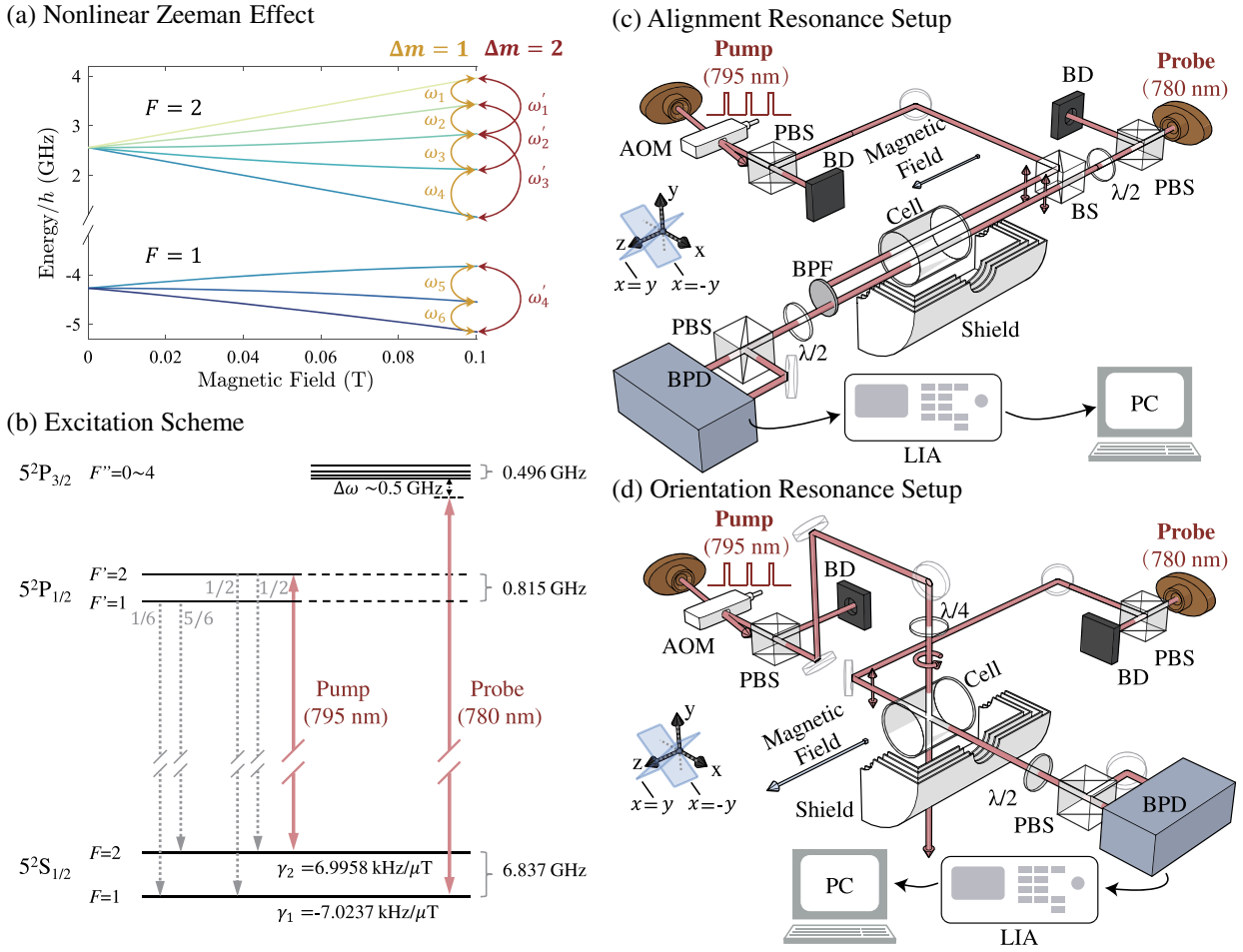

FIG. 1. Schematic of NLZ-heading-error-free magnetometer. (a) Nonlinear Zeeman effect of the ^{87}Rb ground state $5^2S_{1/2}$ and corresponding magnetic resonance frequencies. In the $F = 2$ ($F = 1$) hyperfine state, there are four (two) different $\Delta m = 1$ magnetic resonance frequencies, labeled from ω_1 to ω_4 (ω_5 to ω_6), respectively, and three (one) different $\Delta m = 2$ magnetic resonance frequencies, labeled from ω_1' to ω_3' (ω_4'), respectively. (b) Energy levels of ^{87}Rb atoms and its excitation scheme. The pump beam is a 795 nm laser beam exciting the $5^2S_{1/2}F = 2$ to $5^2P_{1/2}F' = 2$ transition, which generates atomic spin polarization in the $5^2S_{1/2}F = 1$ state via repopulation pumping; the probe beam is a 780 nm laser tuned to the low-frequency side relative to the $5^2S_{1/2}F = 1$ to $5^2P_{3/2}F'' = 0$ transition. (c) Alignment resonance setup. Pump: a linearly polarized 795 nm laser beam used to generate the atomic alignment polarization. Probe: a linearly polarized 780 nm laser beam used to detect the Larmor precession of the atomic alignment polarization via optical rotation. AOM: the acousto-optic modulator used to pulse the pump beam. PBS: polarizing beam splitter. BS: beam splitter. $\lambda/2$: half-wave plate. BPD: balanced photodiode. BPF: bandpass filter with central wavelength of 780 nm, which is used to prevent the pump beam from entering the BPD. BD: beam dump. LIA: lock-in amplifier. PC: personal computer. (d) Orientation resonance setup. Pump: a circularly polarized 795 nm laser beam used to generate the atomic orientation polarization. Probe: a linearly polarized 780 nm laser beam used to detect the Larmor precession of the atomic orientation polarization via optical rotation. $\lambda/4$: quarter-wave plate. Other labels are the same as those in (c).

power broadening of the magnetic resonances. A $\partial B_z/\partial z$ gradient coil is used to compensate the magnetic field gradient. We find that compensating this gradient is sufficient for the purpose of this Letter. The alignment signal is always a single Lorentzian peak, with the central frequency at $2\omega_L$, corresponding to the $\Delta m = 2$ magnetic resonance between the $F = 1$, $m_F = -1$ and $F = 1$, $m_F = 1$ states, while the orientation signal consists of two peaks with increased splitting as the magnetic field is increased. Both the alignment and orientation resonances slightly broaden at stronger magnetic fields due to residual magnetic gradients.

When the magnetic field is not along the z direction, the relative heights of the two Lorentzian peaks in the orientation magnetic resonance are dependent on the magnetic field direction, which leads to an asymmetry and a central-frequency shift of the magnetic resonance [see Figs. S1(c) and S1(d) in the Supplemental Material [37]]. This gives rise to the NLZ-related heading error. In contrast, the alignment resonance is always symmetric [see Figs. S1(a)

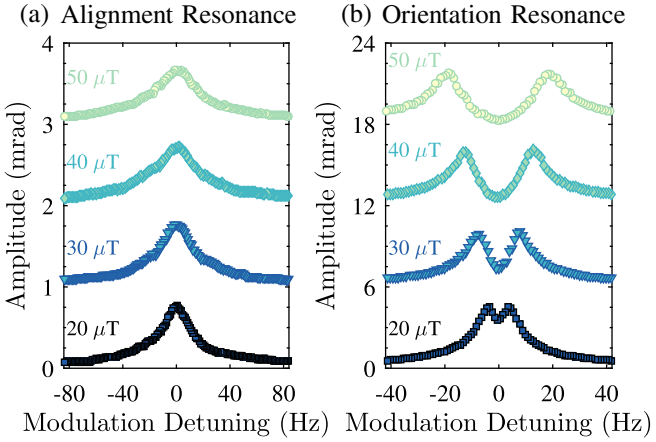

FIG. 2. Magnetic resonances of alignment and orientation polarization with background magnetic fields of different strengths. (a) Alignment resonance. (b) Orientation resonance. The background magnetic field is set along the z direction, with strength ranging from 20 μT to 50 μT. Different magnetic resonances are shifted vertically for clarity. Since the alignment-resonance frequency is about twice that of the orientation resonance, the scale of detuning in (a) is also twice that of (b). The amplitude of the alignment signal is smaller than that of the orientation signal for the reasons explained in Ref. [40].

and S1(b) in the Supplemental Material [37]]. This means that magnetometry based on this alignment resonance is free from the NLZ-related heading error.

In the geomagnetic field range, the estimated photon-shot-noise-limited sensitivities [41–45] of the alignment-based magnetometry are in the tens of $\mathrm{fT}/\sqrt{\mathrm{Hz}}$ range [see Fig. S3(a) in the Supplemental Material [37]]. The best sensitivity is about 9 $\mathrm{fT}/\sqrt{\mathrm{Hz}}$. When the background field gets larger, there is a degradation of the sensitivity. One possible reason for this is the increased magnetic field gradient.

Another source of heading error comes from the different Larmor frequencies of the $F = 1$ and $F = 2$ hyperfine states (≈27.9 Hz/μT; it is in the kHz range in geomagnetic fields), as the tails of the nearby $F = 2$ resonance that change in size depending on the magnetic field direction introduce direction-related error to the measurement of the $F = 1$ Larmor frequency. Taking a resonance at 20 μT, for example (Fig. S2 in the Supplemental Material [37]), the $F = 1$ Larmor frequency can be determined from either the peak frequency of the demodulated X signal or the zero-crossing frequency of the demodulated Y signal. These frequencies, however, are shifted by the $F = 2$ resonance, because the X (Y) contribution from the $F = 2$ resonance leads to a sloping background (residual background) around the $F = 1$ resonance frequency. As the efficiency of producing and detecting atomic spin polarization is dependent on the orientation of the pump or probe laser beam relative to the magnetic field, the $F = 2$ resonance amplitude depends on the field direction as well, thus leading to heading error. Reducing the relative amplitude of the $F = 2$ resonance is beneficial for reducing its tails around the $F = 1$ resonance and the consequent heading error. Due to the fully resolved ground hyperfine states, the probe beam is far detuned from the transitions involving the undesired $5^2S_{1/2}F = 2$ state, suppressing the amplitude of the $F = 2$ resonance to about $1/100$ of the $F = 1$ resonance [see Fig. S2 in the Supplemental Material [37]]. Considering the large frequency difference between these two resonances, the influence from the $F = 2$ resonance on the $F = 1$ Larmor frequency only leads to heading error on the order of tens of fT [see Supplemental Material [37]].

The light shift due to the probe beam is also a source of error. When the background magnetic field is not aligned with the polarization of the probe beam, this beam generally contains π component together with the σ^+ and σ^-. As the light shifts of the $F = 1, m = -1$ and $F = 1, m = 1$ states are almost identical, the shift of the alignment resonance (corresponding to the transition between the $F = 1, m = -1$ and $F = 1$, $m = 1$ states) is largely suppressed [46]. However, there is still residual shift due to the Zeeman-effect-related unbalanced detuning of optical transitions involving, respectively, the $F = 1$, $m = 1$ and $F = 1, m = -1$ states, which is on the order of several pT, according to simulations based on the ADM package [47]. If the polarization of the probe beam is actively rotated to keep it perpendicular to the magnetic field, the light shift will only lead to a constant bias, rather than a heading error. This method also helps in building a dead-zone-free magnetometer [48]. In principle, there may also exist systematic effects due to interference effects including those mediated by radiative polarization transfer [49,50]. The presence of such effects can be identified by measuring the heading error as a function of the light power (particularly, the pump power) and eliminated using a "free-decay" protocol, where atomic evolution occurs in the absence of applied light between pump and probe light pulses.

To conclude, we demonstrated a simple-to-implement (not requiring application of additional fields or modulations), sensitive, heading-error-free scalar magnetometer which can work in geomagnetic environment. This magnetometer is based on the $\Delta m = 2$ magnetic resonance in the ^{87}Rb $F = 1$ ground hyperfine state. In contrast to conventional alkali-metal magnetometry, where the magnetic resonance curve is split and distorted in the geomagnetic field, the resonance demonstrated here is a single Lorentzian, free from NLZ-induced splitting and asymmetry. For our magnetometer, photon-shot-noise-limited sensitivity can reach 9 $\mathrm{fT}/\sqrt{\mathrm{Hz}}$, with the vapor cell at room temperature. The sensitivity can be further improved by heating the cell to increase atomic-vapor density [51]. This scheme is also effective at suppressing the heading error due to the NuZ and LS effects. Due to the fully resolved ground hyperfine states in the antirelaxation-coated cell, the

residual signal from $F = 2$ is relatively small, and thus its influence is at most at the tens of fT level, which is at the limit of the sensitivity of this magnetometer for 1 Hz bandwidth. Moreover, as only linearly polarized light is used, the vector light shift is also largely suppressed [46], which is another possible source of heading error. Considering that the remaining tensor light shift will not change the frequency difference between $m = \pm 1$ magnetic sublevels in the ground $F = 1$ system—i.e., the central frequency of the desired $\Delta m = 2$ magnetic resonance—this scheme is promising for more accurate magnetometry. It should be noted that though the $\Delta m = 2$ magnetic resonance is free from NLZ-induced splitting and asymmetry, the magnetic resonance frequency itself still has cubic corrections in the strength of the magnetic field. Finally, a similar method can be implemented with other alkali metals that have a $F = 1$ ground level, such as ^{39}K, ^{41}K and ^{23}Na.

The authors thank Brian B. Patton, Simon M. Rochester, Sheng Li, Oleg Tetriak, and D. C. Hovde for helpful discussions. This work was supported in part by DFG Project ID No. 390831469: EXC 2118 (PRISMA + Cluster of Excellence), the European Research Council (ERC) under the European Union Horizon 2020 Research and Innovation Program (Grant Agreement No. 695405), the DFG Reinhart Koselleck Project, and the German Federal Ministry of Education and Research (BMBF) within the Quantumtechnologien program (FKZ No. 13N15064). R. Z. acknowledges support from the China Scholarship Council (CSC) enabling his research at the Helmholtz-Institut Mainz and thanks Wei Xiao, Xiang Peng, and Teng Wu for proofreading the manuscript. D. K. acknowledges Martin Engler's help with the LabVIEW code.

*hongguo@pku.edu.cn
†budker@uni-mainz.de

[1] E. Friis-Christensen, H. Lühr, and G. Hulot, Swarm: A constellation to study the earth's magnetic field, Earth Planets Space **58**, 351 (2006).
[2] C. R. de Souza Filho, A. R. Nunes, E. P. Leite, L. V. S. Monteiro, and R. P. Xavier, Spatial analysis of airborne geophysical data applied to geological mapping and mineral prospecting in the Serra Leste region, Carajás mineral province, Brazil, Surv. Geophys. **28**, 377 (2007).
[3] R. Parker, A. Ruffell, D. Hughes, and J. Pringle, Geophysics and the search of freshwater bodies: A review, Sci. Justice **50**, 141 (2010).
[4] V. Pilipenko, O. Kozyreva, M. Engebretson, and A. Soloviev, Ulf wave power index for space weather and geophysical applications: A review, Russian J. Earth Sci. **17**, 1 (2017).
[5] D. Murzin, D. J. Mapps, K. Levada, V. Belyaev, A. Omelyanchik, L. Panina, and V. Rodionova, Ultrasensitive magnetic field sensors for biomedical applications, Sensors **20**, 1569 (2020).
[6] K.-M. C. Fu, G. Z. Iwata, A. Wickenbrock, and D. Budker, Sensitive magnetometry in challenging environments, AVS Quantum Sci. **2**, 044702 (2020).
[7] M. S. Safronova, D. Budker, D. DeMille, D. F. J. Kimball, A. Derevianko, and C. W. Clark, Search for new physics with atoms and molecules, Rev. Mod. Phys. **90**, 025008 (2018).
[8] M. A. Fedderke, P. W. Graham, D. F. Jackson Kimball, and S. Kalia, Earth as a transducer for dark-photon dark-matter detection, Phys. Rev. D **104**, 075023 (2021).
[9] M. A. Fedderke, P. W. Graham, D. F. Jackson Kimball, and S. Kalia, Search for dark-photon dark matter in the supermag geomagnetic field dataset, Phys. Rev. D **104**, 095032 (2021).
[10] A. Arza, M. A. Fedderke, P. W. Graham, D. F. Jackson Kimball, and S. Kalia, Earth as a transducer for axion dark-matter detection, Phys. Rev. D **105**, 095007 (2022).
[11] T. E. Chupp, P. Fierlinger, M. J. Ramsey-Musolf, and J. T. Singh, Electric dipole moments of atoms, molecules, nuclei, and particles, Rev. Mod. Phys. **91**, 015001 (2019).
[12] D. F. Jackson Kimball, J. Dudley, Y. Li, D. Patel, and J. Valdez, Constraints on long-range spin-gravity and monopole-dipole couplings of the proton, Phys. Rev. D **96**, 075004 (2017).
[13] Z. Wang, X. Peng, R. Zhang, H. Luo, J. Li, Z. Xiong, S. Wang, and H. Guo, Single-Species Atomic Comagnetometer Based on ^{87}Rb Atoms, Phys. Rev. Lett. **124**, 193002 (2020).
[14] P. G. Park, Y. G. Kim, V. Y. Shifrin, and V. N. Khorev, Precise standard system for low dc magnetic field reproduction, Rev. Sci. Instrum. **73**, 3107 (2002).
[15] V. Shifrin, V. Khorev, V. Kalabin, and P. Park, Experimental estimation of the accuracy of modern scalar quantum magnetometers in measurements of the Earth's magnetic field, Phys. Earth Planet. Inter. **166**, 147 (2008).
[16] D. Sheng, S. Li, N. Dural, and M. V. Romalis, Subfemtotesla Scalar Atomic Magnetometry Using Multipass Cells, Phys. Rev. Lett. **110**, 160802 (2013).
[17] D. F. J. Kimball and D. Budker, *Optical Magnetometry* (Cambridge University Press, Cambridge, England, 2013).
[18] D. Budker and M. G. Kozlov, Sensing: Equation one, arXiv:2011.11043.
[19] V. G. Lucivero, W. Lee, N. Dural, and M. V. Romalis, Femtotesla Direct Magnetic Gradiometer Using a Single Multipass Cell, Phys. Rev. Appl. **15**, 014004 (2021).
[20] V. G. Lucivero, W. Lee, M. E. Limes, E. L. Foley, T. W. Kornack, and M. V. Romalis, Femtotesla Nearly-Quantum-Noise-Limited Pulsed Gradiometer at Earth-Scale Fields, Phys. Rev. Appl. **18**, L021001 (2022).
[21] S. Groeger, A. Pazgalev, and A. Weis, Comparison of discharge lamp and laser pumped cesium magnetometers, Appl. Phys. B **80**, 645 (2005).
[22] G. Bao, A. Wickenbrock, S. Rochester, W. Zhang, and D. Budker, Suppression of the Nonlinear Zeeman Effect and Heading Error in Earth-Field-Range Alkali-Vapor Magnetometers, Phys. Rev. Lett. **120**, 033202 (2018).
[23] G. Oelsner, V. Schultze, R. IJsselsteijn, F. Wittkämper, and R. Stolz, Sources of heading errors in optically pumped magnetometers operated in the Earth's magnetic field, Phys. Rev. A **99**, 013420 (2019).

[24] W. Lee, V. G. Lucivero, M. V. Romalis, M. E. Limes, E. L. Foley, and T. W. Kornack, Heading errors in all-optical alkali-metal-vapor magnetometers in geomagnetic fields, Phys. Rev. A **103**, 063103 (2021).
[25] Y. Chang, Y.-H. Guo, S.-A. Wan, and J. Qin, Nuclear Zeeman Effect on Heading Errors and the Suppression in Atomic Magnetometers, arXiv:2102.03037.
[26] A. Mozers, L. Busaite, D. Osite, and M. Auzinsh, Angular momentum alignment-to-orientation conversion in the ground state of Rb atoms at room temperature, Phys. Rev. A **102**, 053102 (2020).
[27] D. Budker, D. F. Kimball, S. M. Rochester, and V. V. Yashchuk, Nonlinear Magneto-Optical Rotation via Alignment-to-Orientation Conversion, Phys. Rev. Lett. **85**, 2088 (2000).
[28] K. Jensen, V. M. Acosta, J. M. Higbie, M. P. Ledbetter, S. M. Rochester, and D. Budker, Cancellation of nonlinear Zeeman shifts with light shifts, Phys. Rev. A **79**, 023406 (2009).
[29] In some cases, heading errors due to NuZ [24] or LS [23] effects are suppressed together with the NLZ-related effect at the same time.
[30] S. J. Seltzer, P. J. Meares, and M. V. Romalis, Synchronous optical pumping of quantum revival beats for atomic magnetometry, Phys. Rev. A **75**, 051407(R) (2007).
[31] A. Ben-Kish and M. V. Romalis, Dead-Zone-Free Atomic Magnetometry with Simultaneous Excitation of Orientation and Alignment Resonances, Phys. Rev. Lett. **105**, 193601 (2010).
[32] G. Bao, D. Kanta, D. Antypas, S. Rochester, K. Jensen, W. Zhang, A. Wickenbrock, and D. Budker, All-optical spin locking in alkali-metal-vapor magnetometers, Phys. Rev. A **105**, 043109 (2022).
[33] V. M. Acosta, M. Auzinsh, W. Gawlik, P. Grisins, J. M. Higbie, D. F. J. Kimball, L. Krzemien, M. P. Ledbetter, S. Pustelny, S. M. Rochester, V. V. Yashchuk, and D. Budker, Production and detection of atomic hexadecapole at Earth's magnetic field, Opt. Express **16**, 11423 (2008).
[34] S. Pustelny, M. Koczwara, L. Cincio, and W. Gawlik, Tailoring quantum superpositions with linearly polarized amplitude-modulated light, Phys. Rev. A **83**, 043832 (2011).
[35] D. A. Steck, Rubidium 87 D line data, [EB/OL] (2010), avalible online at http://steck.us/alkalidata (revision 2.1.4, 2010).
[36] W. Happer, Optical pumping, Rev. Mod. Phys. **44**, 169 (1972).
[37] See Supplemental Material at http://link.aps.org/supplemental/10.1103/PhysRevLett.130.153601 for details about magnetic-field-direction dependence of alignment and orientation resonances, estimation of nuclear-Zeeman-effect-related heading error, and sensitivity estimation.
[38] W. Chalupczak, R. M. Godun, S. Pustelny, and W. Gawlik, Room temperature femtotesla radio-frequency atomic magnetometer, Appl. Phys. Lett. **100**, 242401 (2012).
[39] R. Gartman and W. Chalupczak, Amplitude-modulated indirect pumping of spin orientation in low-density cesium vapor, Phys. Rev. A **91**, 053419 (2015).
[40] M. Auzinsh, D. Budker, and S. M. Rochester, Light-induced polarization effects in atoms with partially resolved hyperfine structure and applications to absorption, fluorescence, and nonlinear magneto-optical rotation, Phys. Rev. A **80**, 053406 (2009).
[41] D. Budker, D. F. Kimball, S. M. Rochester, V. V. Yashchuk, and M. Zolotorev, Sensitive magnetometry based on nonlinear magneto-optical rotation, Phys. Rev. A **62**, 043403 (2000).
[42] V. Acosta, M. P. Ledbetter, S. M. Rochester, D. Budker, D. F. Jackson Kimball, D. C. Hovde, W. Gawlik, S. Pustelny, J. Zachorowski, and V. V. Yashchuk, Nonlinear magneto-optical rotation with frequency-modulated light in the geophysical field range, Phys. Rev. A **73**, 053404 (2006).
[43] E. Zhivun, Vector AC Stark shift in ^{133}Cs atomic magnetometers with antirelaxation coated cells, Ph.D. thesis, University of California, Berkeley, Berkeley, CA, USA, 2016.
[44] C. Troullinou, R. Jiménez-Martínez, J. Kong, V. G. Lucivero, and M. W. Mitchell, Squeezed-Light Enhancement and Backaction Evasion in a High Sensitivity Optically Pumped Magnetometer, Phys. Rev. Lett. **127**, 193601 (2021).
[45] V. G. Lucivero, P. Anielski, W. Gawlik, and M. W. Mitchell, Shot-noise-limited magnetometer with sub-picotesla sensitivity at room temperature, Rev. Sci. Instrum. **85**, 113108 (2014).
[46] F. Le Kien, P. Schneeweiss, and A. Rauschenbeutel, Dynamical polarizability of atoms in arbitrary light fields: General theory and application to cesium, Eur. Phys. J. D **67**, 92 (2013).
[47] AtomicDensityMatrix, [EB/OL], http://rochesterscientific.com/ADM/ Accessed 2022.
[48] T. Wu, X. Peng, Z. Lin, and H. Guo, A dead-zone free ^{4}He atomic magnetometer with intensity-modulated linearly polarized light and a liquid crystal polarization rotator, Rev. Sci. Instrum. **86**, 103105 (2015).
[49] M. Horbatsch and E. A. Hessels, Shifts from a distant neighboring resonance, Phys. Rev. A **82**, 052519 (2010).
[50] A. Marsman, M. Horbatsch, and E. A. Hessels, Interference between two resonant transitions with distinct initial and final states connected by radiative decay, Phys. Rev. A **96**, 062111 (2017).
[51] W. Li, M. Balabas, X. Peng, S. Pustelny, A. Wickenbrock, H. Guo, and D. Budker, Characterization of high-temperature performance of cesium vapor cells with anti-relaxation coating, J. Appl. Phys. **121**, 063104 (2017).